
Working Memory Graphs

Ricky Loynd, Roland Fernandez, Asli Celikyilmaz, Adith Swaminathan & Matthew Hausknecht

Microsoft Research AI

{riloynd,rfernand,aslice1,adswamin,mahauskn}@microsoft.com

Abstract

Transformers have increasingly outperformed gated RNNs in obtaining new state-of-the-art results on supervised tasks involving text sequences. Inspired by this trend, we study the question of how Transformer-based models can improve the performance of sequential decision-making agents. We present the Working Memory Graph (WMG), an agent that employs multi-head self-attention to reason over a dynamic set of vectors representing observed and recurrent state. We evaluate WMG in three environments featuring factored observation spaces: a Pathfinding environment that requires complex reasoning over past observations, BabyAI gridworld levels that involve text instructions, and Sokoban which emphasizes future planning. We find that the combination of WMG’s Transformer-based architecture with factored observation spaces leads to significant gains in learning efficiency compared to other architectures across all tasks. Our results imply that for environments where it is possible to factorize environment observations, WMG’s Transformer-based architecture can dramatically boost sample efficiency.

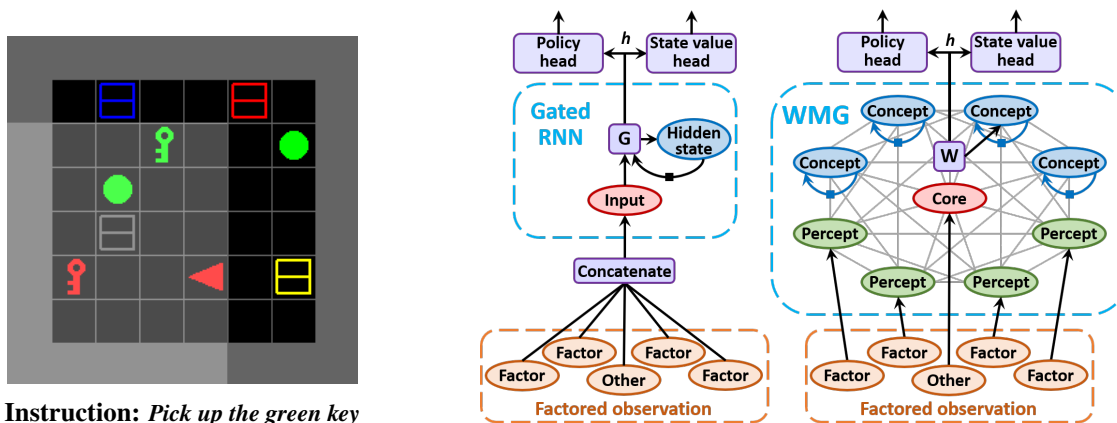
1. Introduction

Because of their ability to process sequences of data, gated Recurrent Neural Networks (RNNs) have been widely applied to natural language processing (NLP) tasks such as machine translation. In the RNN-based approach of Sutskever et al. (2014), an encoder RNN maps an input sentence in the source language to a series of internal hidden state vectors. The encoder’s final hidden state is copied into a decoder RNN, which then generates another sequence of hidden states that determine the selection of output tokens in the target language. This model can be trained to translate sentences, but translation quality deteriorates on long sentences where long-term dependencies become critical. A widely-held conjecture for this drop in performance attributes it to the limited representational capacity of RNN’s hidden

state vectors. In Bahdanau et al. (2014), translation quality is boosted by applying an attention mechanism to create paths serving as shortcuts from the input to the output sequences, routing information outside the linear chain of the RNN’s hidden states. Similar attention mechanisms have since gained wide usage, culminating in the Transformer model (Vaswani et al., 2017) which replaces the RNN with many short paths of self-attention. Since then, Transformers have outperformed RNNs on many NLP tasks (Devlin et al., 2018; Dong et al., 2019; Liu et al., 2019).

We seek to leverage these intuitions to improve the ability of Reinforcement Learning (RL) agents to reason over long time horizons in Partially Observable Markov Decision Processes (POMDPs) (Kaelbling et al., 1998). In a POMDP, a single observation Obs_t is not sufficient to identify the latent environment state s_t . Thus the agent must reason over the history of past observations in order to select the best action for the current step. A simple strategy employed by DQN (Mnih et al., 2015) is to condition the policy on the N most recent observations $\pi(a_t|Obs_{t-N+1} \dots Obs_t)$. But in complex environments, the sufficient number N may be large, highly variable, and unknown. To address this issue, gated RNNs such as LSTMs (Hochreiter & Schmidhuber, 1997) and GRUs (Chung et al., 2015) use internal, recurrent state vectors which in theory can maintain information from past observations (Hausknecht & Stone, 2015; Oh et al., 2016). However, in practice, these methods are limited by the single path of information flow defined by the linear chain of RNN hidden states. As in NLP, we hypothesize that providing alternative paths for information will be advantageous to RL agents. Building on this intuition, we introduce the Working Memory Graph (WMG), a Transformer-based agent that uses self-attention to provide a multitude of shortcut paths for information to flow between past observations and the current action. This is enabled by a dynamic set of hidden state vectors, called *Concepts* illustrated in Figure 1 (right), which preserve information through time and form the basis for WMG to flexibly reason over past observations.

Motivated by prior work on factored representations (Russell & Norvig, 2009) and factored MDPs (Boutillier et al., 2000; 2001), we argue that factored observations are ideally suited for input to Transformer-based agents like WMG.



Instruction: Pick up the green key

Figure 1. **Left:** BabyAI rewards the agent (red triangle) for performing the task given by the instruction. **Right:** Comparing a gated RNN agent to WMG: a gated RNN constrains information to flow through time in a linear path of hidden state vectors, whereas WMG allows information to flow through many self-attention paths among the set of *Concept* vectors. *Percept* vectors embed observation factors and are used along with *Concepts* as input to WMG’s multi-layer Transformer W .

Although many environments use fixed-sized feature spaces, certain environments have observations amenable to factorization. As a motivating example, consider the BabyAI environment (Chevalier-Boisvert et al., 2018) as depicted in Figure 1 (left). The native observation space includes the agent’s field of view, a 7×7 grid, shown in lighter grey. This observation can be efficiently represented by a set of factors describing the types, colors, and relative x and y coordinates of all visible objects: ([green, key, 1, 3], [grey, box, 2, 1], [green, ball, 2, 2], [red, key, 3, 0]). This *factored observation* is more compact than the native observation, but will vary in size depending on the number of objects in view. Individual factors of the observation (e.g. [grey, box, 2, 1]) are embedded into *Percept* vectors (Fig. 1 right) which serve as input to WMG’s Transformer, along with the *Concept* vectors that WMG maintains.

Our contributions are twofold: First we introduce the *Working Memory Graph* (WMG), a Transformer-based agent implementing a novel form of *shortcut recurrence* which we demonstrate to be effective at complex reasoning over long-term dependencies. Second, we identify the synergy between Transformer-based RL architectures and *factored observations*, demonstrating that by virtue of self-attention, WMG is able to effectively leverage factored observations to learn high-performing policies using fewer environment interactions than alternative architectures.

2. Related Approaches

Prior approaches for reasoning over long time horizons have used attention for memory access (Graves et al., 2016; Oh et al., 2016) or self-attention to process individual observations (Zambaldi et al., 2019; Vinyals et al., 2019). These

approaches all used LSTM-based recurrence over time. In contrast, WMG obviates the need for gated recurrence by applying self-attention to a network of *Concept* vectors which are persisted through time.

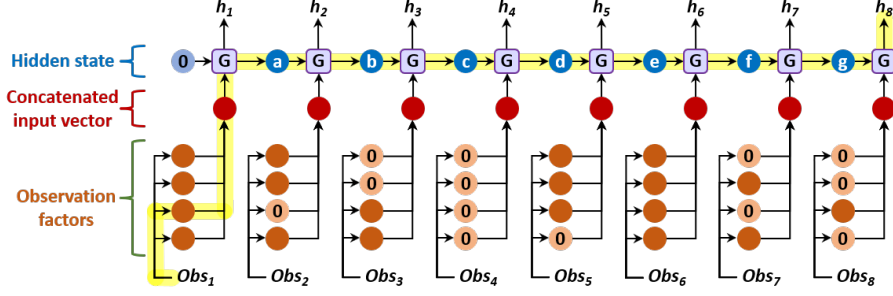
Other Transformer-based models handle partial observability using state vectors analogous to WMG’s *Concepts*, but with different state-update schedules: RMC (Santoro et al., 2018) updates all state vectors on every time step, while RIMs (Goyal et al., 2019) enforces sparsity by updating exactly half of the state vectors on each step. In contrast to RMC and RIMs which update a large proportion of their recurrent state vectors at each step, WMG replaces only one *Concept* on each time step in order to maximize the persistence of latched *Concept* vectors, thereby allowing it to preserve information through time.

Unlike the other models discussed here, the Gated Transformer-XL (Anonymous, 2019) addresses partial observability by feeding hundreds of past observations at once into the Transformer. In contrast, in order to mitigate the $O(N^2)$ computational cost of self-attention, WMG computes self-attention over a comparatively small number of *Concept* vectors to capture and maintain the relevant aspects of past observations.

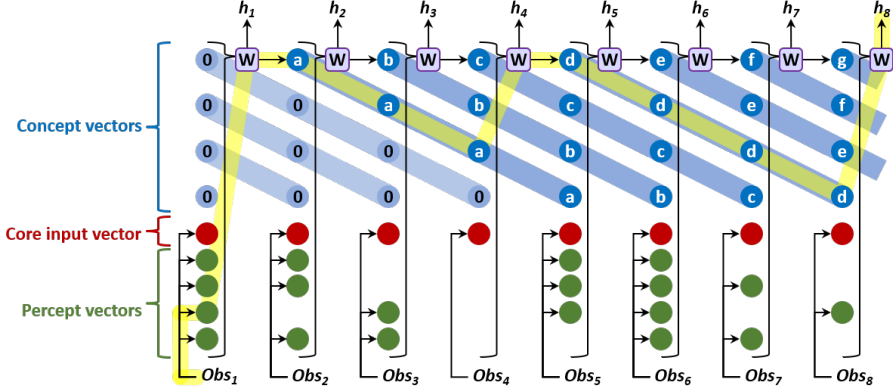
3. Working Memory Graph

The term *Working Memory Graph* is motivated by the *limited* size of WMG’s self-attention computation graph, in loose analogy with the cognitive science term *working memory*, which refers to a cognitive system that holds a limited amount of information for use in mental processing (Miller, 1956). As illustrated in Figure 1, WMG applies multi-head

Working Memory Graphs



(a) Gated RNN unrolled in time.



(b) WMG unrolled in time.

Figure 2. Unrolled Over Time: In a Gated RNN, for the first observation Obs_1 to affect the agent’s output h_8 , information must pass through 8 gating operations and 7 intervening hidden states **a-g**. In contrast, in a WMG, many possible paths lead from the first observation to the output h_8 . The highlighted path requires only three passes through **W**, as the information is first stored for several time steps in Concept **a** and later in Concept **d**. This example illustrates one of many possible shortcut paths for information to flow forward and gradients to flow backward.

self-attention to a dynamic set of hidden state vectors, the *Concepts*, which store information from previous timesteps. Formally, each Concept vector defines one row in a Concept matrix $C \in \mathbb{R}^{n_C \times d_C}$, where n_C is the number of Concepts maintained by WMG and d_C is the dimension of each Concept vector. Once created, a Concept vector persists unchanged through time and on each time step, the oldest Concept is replaced by a new one. For example, in Figure 2 the Concept vector b is created at step 2 and persists unchanged for 4 timesteps before being overwritten with Concept f after step 6. These Concepts form the basis of WMG’s *shortcut recurrence*, which replaces a gated RNN’s single path of information flow with a network of shorter self-attention paths.

Beyond Concepts, WMG also applies self-attention to variably-sized factored observations using *Percept* vectors, depicted in green in Figures 1, 2. On each time step, WMG receives a factored observation consisting of a variable number of factors, which are embedded into (n_P) Percept vectors forming a Percept matrix $P \in \mathbb{R}^{n_P \times d_P}$. Finally a core vector $c \in \mathbb{R}^{d_c}$ encodes any global information such as the

text instructions in BabyAI. The core, Percept and Concept vectors are stacked into a matrix for WMG’s Transformer:

$$T^{in} = \begin{bmatrix} cW_{core} + b_{core} \\ PW_{per} + b_{per} \\ C'W_{con} + b_{con} \end{bmatrix}, \quad C' = [C \ I]$$

where $W_{core} \in \mathbb{R}^{d_c \times d_T}$, $W_{per} \in \mathbb{R}^{d_P \times d_T}$ and $W_{con} \in \mathbb{R}^{(d_C + n_C) \times d_T}$ are embedding matrices with corresponding bias vectors $b \in \mathbb{R}^{d_T}$ broadcast over rows. Each Concept is concatenated with a one-hot vector indicating its age. Closely following the encoder architecture of Vaswani et al. (2017), WMG’s Transformer operation takes the input matrix $T^{in} \in \mathbb{R}^{n_T \times d_T}$ and returns an output matrix $T^{out} \in \mathbb{R}^{n_T \times d_T}$, where $n_T = 1 + n_P + n_C$ is the number of input (or output) nodes, and d_T is the size of each node vector. The oldest Concept (denoted here by the first row of the Concept matrix, the remaining rows of the matrix denoted by $C_{-n_C, :}$) is replaced by a new Concept vector generated as a non-linear function of the core node’s output

vector $\mathbf{h} = \mathbf{T}_{1,:}^{out}$:

$$\mathbf{C} = \begin{bmatrix} \tanh(\mathbf{h}\mathbf{W}_C + \mathbf{b}_C) \\ \mathbf{C}_{-n_C} \end{bmatrix}, \mathbf{W}_C \in \mathbb{R}^{d_T \times d_C}, \mathbf{b}_C \in \mathbb{R}^{d_C}$$

RL Training. The trainable parameters θ of WMG and its Transformer layers are trained end-to-end through backpropagation of the standard policy-gradient loss maximizing the cumulative expected return $\mathcal{J}(\theta)$:

$$\nabla_{\theta} \mathcal{J}(\theta) = \mathbb{E}_{\pi} \left[\sum_{t=0}^{\infty} \nabla_{\theta} \log \pi(a_t | \mathbf{h}_t; \theta) A^{\pi}(Obs_t, a_t) + \beta \nabla_{\theta} H(\pi(\mathbf{h}_t; \theta)) \right]$$

where $\pi(a | \mathbf{h}_t; \theta)$ denotes WMG’s policy head operating on hidden state \mathbf{h}_t (see Fig. 1 right), H is the entropy of the policy’s action distribution, and β controls the strength of the entropy regularization term. When performing backpropagation through time, the maximum number of steps for gradient flow backwards through time is denoted by t_{max} . To reduce the variance of gradient estimates, we use the advantage actor-critic algorithm described by Mnih et al. (2016), which estimates the advantage $A^{\pi}(s_t, a_t)$ using a γ -discounted k -step return as follows:

$$A^{\pi}(Obs_t, a_t) = \left(\sum_{i=0}^{k-1} \gamma^i r_{t+i} \right) + \gamma^k V^{\pi}(\mathbf{h}_{t+k}) - V^{\pi}(\mathbf{h}_t; \theta)$$

where $V(\mathbf{h}_t; \theta)$ denotes WMG’s state-value head (see Fig. 1 right), which is trained to minimize the squared difference between the k -step return and the current value estimate: $\|(\sum_{i=0}^{k-1} \gamma^i r_{t+i} + \gamma^k V^{\pi}(\mathbf{h}_{t+k})) - V(\mathbf{h}_t)\|^2$, and k is upper-bounded by the number of time steps (t_{max}) in the actor’s current update window.

4. Experiments

Our experiments aim to (1) evaluate WMG’s ability to reason over long time spans in a setting of high partial observability, and (2) understand how factored representations may be effectively utilized by WMG. To address these questions we present results on three diverse environments: a novel Pathfinding task which requires complex reasoning over past observations, the BabyAI domain (Chevalier-Boisvert et al., 2018) which involves changing goals, partial observability, and textual instructions, and Sokoban (Guez et al., 2019) a challenging puzzle environment that benefits from forward planning ability. To foreshadow our results, the Pathfinding task demonstrates the effectiveness of WMG’s shortcut recurrence, BabyAI demonstrate that WMG leverages factored observations to deliver substantial gains in sample efficiency, while Sokoban shows that WMG is capable of handling highly complex tasks. These experimental results illustrate WMG’s ability to handle highly diverse and

complex tasks, as long as their observations are amenable to factorization.

4.1. Pathfinding Task

The Pathfinding task is designed to evaluate WMG’s ability to perform complex reasoning over past observations. Figure 3 depicts the incremental construction of a directed graph over nodes identified by unique pattern vectors which are randomly generated on every episode. (See Appendix A for the graph-construction algorithm and other details.) On odd time steps the agent observes two pattern nodes to be linked, and on even steps the agent must indicate whether or not a directed path exists from one given pattern to another. As this cycle repeats, the graph grows larger and the agent must perform an increasing number of reasoning steps to confirm or deny the existence of a path between arbitrary nodes. Because the observation only contains incremental information and the entirety of the graph is never directly observed, the agent must leverage information from previous observations to infer connectivity between nodes.

For example, consider step 4 of Figure 3: To determine whether a path exists from green to yellow, the agent must recall and combine information from steps 1 and 3. Similarly, on step 12, if the agent were asked about the existence of a path from cyan to yellow, answering correctly without guessing would require piecing together information from three non-contiguous time steps. Since the actual quiz on step 12 asks whether a path exists from green to blue, the agent must reason over many past observations to determine that no such path exists.

Each pattern is a vector of D real numbers drawn randomly from the interval -1 to 1 . A binary value is added to the observation vector to indicate whether the current step is a quiz step, bringing the size of the observation space to $2D + 1$, where $D = 7$ for our experiments. The action space consists of two actions, defined as *yes* or *no*. If the agent answers correctly on a quiz step, it receives a reward of 1; otherwise, it receives a reward of 0. The quiz questions are constructed to guarantee that each answer (*yes* or *no*) is correct half the time, so agents that act randomly or have no memory will obtain 50% of possible reward in expectation.

WMG is configured with Concept nodes to handle the partial observability but no Percept nodes, since we are not using this task to explore factored observations. The number of Concept nodes is a tuned hyperparameter, equal to 16 in this experiment. (See Table D for all settings.) Each observation is passed directly to WMG’s core node, and WMG generates a new Concept on each time step. We compare WMG’s performance to several baselines. Each *Depth- n* baseline is a hand-coded algorithm demonstrating the performance obtained using perfect memory of past observations and reasoning over paths up to n steps long.

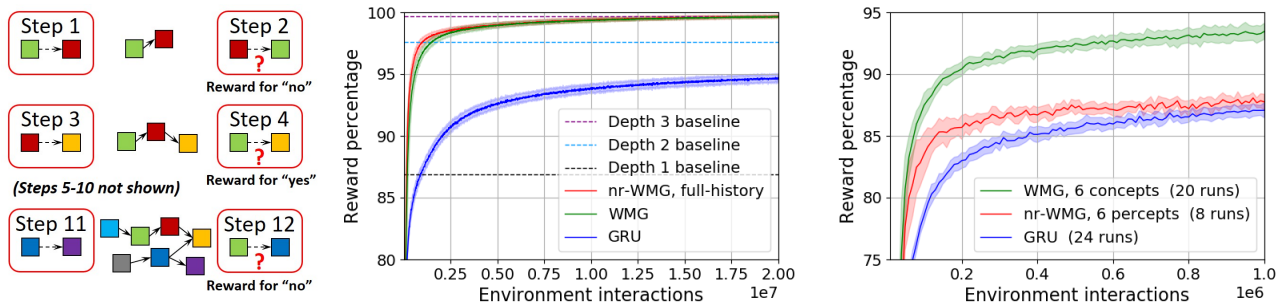


Figure 3. **Left: Pathfinding task**, consists of 12 time steps with a maximum graph size $N = 7$ patterns. The boxes with rounded corners illustrate the observations for the given time steps, where a question mark identifies the step as a quiz step rather than a construction step. The box colors represent distinct pattern vectors. **Middle: Results on Pathfinding**: Each plotted point is the percentage of reward on quiz steps received by the agent over the previous 10k time steps, averaged over 100 independent training runs. Bands display one standard deviation. (See Table 11 for more details.) **Right: WMG restricted to only 6 Concepts** outperforms nr-WMG with access to the last 6 observations as well as GRU.

For example, *Depth-2* remembers all previous construction steps, and reasons over all paths of depth 2. Finally, in order to understand the effectiveness of Concept nodes at capturing past information, we evaluate a *full-history*, non-recurrent version of WMG (nr-WMG) by removing the Concept nodes and giving it all past observations on each time step, each one passed to a separate Percept node.

As shown in Figure 3 (middle), the GRU-based agent exceeds *Depth-1* performance, but remains well short of *Depth-2* performance after 20 million steps of training (environment interactions). In contrast, both versions of the WMG agent nearly reach *Depth-3* performance, demonstrating a greater ability to perform complex reasoning over past observations. The best performance is achieved by the nr-WMG with full-history, which has no need for recurrence. But the full WMG (with Concepts) is nearly as sample efficient as this perfect-memory baseline. These results indicate that shortcut recurrence enables WMG to learn to store and utilize essential information from past Pathfinding observations in a more effective manner than a GRU.

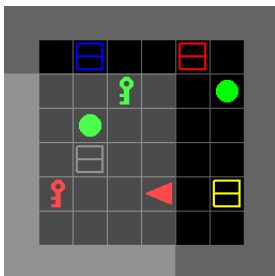
To investigate WMG’s shortcut recurrence, we repeat the Pathfinding experiment while restricting the total number of WMG Concept nodes to 6, which is enough to store only half of the observations in an episode. As shown in Figure 3 (right), limiting WMG to 6 Concepts slightly degrades performance, but it still significantly outperforms nr-WMG which has direct access to the last 6 observations as well as GRU. nr-WMG with 6 Percepts captures the heuristic (employed by DQN (Mnih et al., 2015) etc.) of stacking the previous several observations to combat partial observability. This result suggests that WMG learns to transfer information from older Concepts to newer Concepts in order to reason beyond the last 6 observations and shows that WMG’s shortcut recurrence is more effective than GRU’s linear recurrence.

4.2. BabyAI Environment

In order to understand how factored representations may be effectively utilized by WMG, we study BabyAI, a domain whose observation space is amenable to factorization. BabyAI (Chevalier-Boisvert et al., 2018) is a partially observable, 2D grid-world containing objects that can be viewed and moved by the agent. Unlike most RL environments, BabyAI features text instructions that specify the goal, such as “pick up the green box.”

We focus on five BabyAI levels, for which the environment consists of a single 6x6 room, as shown in Figure 4 (left). Despite the apparent simplicity of a single-room domain, learning to solve it can often take model-free RL agents hundreds of thousands of environment interaction steps (Chevalier-Boisvert et al., 2018). The agent’s action space consists of 7 discrete actions: Move forward, Turn left, Turn right, Pick up, Drop, Toggle, and Done. An episode ends after 64 time steps, or when the agent achieves the goal, for which it receives a reward of 1. In Level 1 (GoToObj), the room contains only one object. The agent completes the mission by moving to an adjacent square and pointing toward the object. In Level 2, the target object is always a red ball, and seven grey boxes are present as distractors. In Level 3, the distractors may be any of the 3 object types and 6 colors. If one of the distractors happens to be a red ball, the agent is rewarded for reaching it. In Level 4, the instruction specifies the color and type of the target object. This is the first level in which the text instruction contains valuable information. (See Table 14 for instruction templates.) Level 5 increases the difficulty of Level 4 in two ways: First, the agent must reach and pickup the target object. Second, if multiple qualifying target objects are present, the agent is given the initial relative location of the true target, such as “behind you”.

Each agent observation in BabyAI consists of a text instruc-



Instruction: Go to the yellow box

Part of observation	Variable assignments	Node
Factored image	color= green , type= key , X=3, Y=1	Percept
Factored image	color= grey , type= box , X=1, Y=2	Percept
Factored image	color= green , type= ball , X=2, Y=2	Percept
Factored image	color= red , type= key , X=0, Y=3	Percept
Factored image	vertical wall X=-2	core
Factored image	horizontal wall Y=4	core
Factored instruction	command= go to , article= the , color= yellow , type= box , loc= None	core
Additional info	orientation= west , last action= move forward	core

Figure 4. One completely factored observation, where each variable assignment corresponds to a one-hot vector in the full observation vector. Since the number of objects in an observation can vary, each object’s vectors are concatenated then passed to a Percept node. All other one-hot vectors from the observation are concatenated then passed to the core node. X & Y coordinates refer to a frame of reference with the agent at the origin, pointed in the positive Y direction. The agent always observes one vertical wall and one horizontal wall.

tion, an image, and the agent’s orientation. The image’s native format is a 7×7 array of cell descriptors (not pixels) identifying three attributes of each cell: type, color, and open/closed/locked (referring to doors, which are not found in these 5 levels). To study factored observations in BabyAI, we define a factored representation, depicted in Figure 4. In our experiments the text instruction is always factored, but the image is formatted in multiple ways: (1) **7x7x3**, the native BabyAI image array; (2) **flat**, the native $7 \times 7 \times 3$ array flattened to one vector; (3) **factored** image, as described in Figure 4. (Note that when a factored image is passed to a GRU, it must first be flattened and padded to form a fixed-length vector.)

To determine whether WMG can leverage factored observations more effectively than gated RNNs in BabyAI, we evaluate the following agents: (1) **WMG** is the full, recurrent WMG model, with Percepts mapped to observation factors, (2) **nr-WMG** is an ablated, non-recurrent version of WMG with no Concepts, (3) **GRU** is a GRU model, and (4) **CNN+GRU** uses a CNN to process the native $7 \times 7 \times 3$ image, followed by a GRU. This CNN is one of the two CNN models provided in the BabyAI open source code (Chevalier-Boisvert et al., 2018).

4.3. BabyAI Results

Factored Observations: The largest performance differences in Table 1 stem from the choice of factored versus flat or native image formats. Notably, WMG with factored images can achieve sample efficiencies 10x greater (on Level 3) than CNN+GRU using the native 7×7 image format. However, factored observations alone are not sufficient for sample efficiency: WMG utilizes factored images much more effectively than a GRU on Levels 2-5. This result supports our hypothesis that Transformer-based models are particularly well suited for operating on set-based inputs like factored observations, and large gains in sample efficiency are observed as a result.

Concept Nodes: Without factored observations, WMG-flat slightly outperforms GRU-flat, suggesting that shortcut recurrence implemented by the WMG’s Concept nodes compares favorably to the GRU’s gated recurrence. With the benefit of factored observations, the non-recurrent ablation of WMG (nr-WMG) performs slightly better than the full WMG on the simplest two levels. But for the more challenging levels 3-5, Concept vectors prove to be of benefit for WMG with factored observations.

Early vs Late instruction fusion: Interestingly, within our training limit of 6 million environment interactions, CNN+GRU is unable to learn to solve the levels (4 & 5) where instructions carry important information. We suspect this is because the CNN processes just the image while the factored instruction is passed directly to the GRU, skipping the CNN. By contrast, the baseline BabyAI agent uses FiLM layers (Perez et al., 2017) to integrate the processing of the image with the text instruction. Both WMG and GRU models can process the image and instruction together in all levels of processing. This early fusion appears to allow all WMG and GRU models to solve Level 4.

In summary, the two WMG models with factored images were the only agents able to solve Level 5, and they learned to do so in approximately the same number of interactions that CNN-GRU required to solve Level 3. These drastic differences in sample efficiency serve to highlight the potential gains that can be achieved by RL agents equipped to utilize factored observations.

While WMG’s sample efficiencies dramatically exceed the RL benchmarks published with the BabyAI domain (Chevalier-Boisvert et al., 2018), often by two orders of magnitude (Table 14), it’s important to note that these sets of results are not directly comparable. Our experiments all used factored text instructions, and each model’s hyperparameters were tuned for each level separately, while the BabyAI benchmark agent was trained on all levels us-

Working Memory Graphs

Model	WMG	nr-WMG	GRU	WMG	GRU	CNN+GRU
Image format	factored	factored	factored	flat	flat	native 7x7x3
1 - GoToObj	1.6	1.4	1.7	15.0	19.0	10.6
2 - GoToRedBallGrey	6.7	5.2	24.6	29.0	31.0	22.3
3 - GoToRedBall	16.0	23.6	174.4	92.0	124.6	204.9
4 - GoToLocal	59.7	71.3	2,241.6	1,379.9	1,799.4	—
5 - PickupLoc	222.3	253.0	—	—	—	—

Table 1. **BabyAI sample efficiency**: the amount of training (shown here in thousands of environment interactions) required for a model to solve 99% of 10,000 episodes. Hyperparameters were first tuned on each model/format/level combination separately, then each reported result was computed as the median sample efficiency over 100 additional training runs. Dashes indicate that no model reliably reached a solution rate of 99% within 6 million training steps (environment interactions). Note that (Chevalier-Boisvert et al., 2018) report sample efficiencies in terms of episodes rather than environment interactions. (See Table 14.)

ing the single hyperparameter configuration provided in the BabyAI release. Because of these differences, our experiments should not be interpreted as a new state-of-the-art on the standard BabyAI tasks.

4.3.1. HYPERPARAMETER SENSITIVITY

To evaluate WMG’s sensitivity to hyperparameter selection, we applied the tuned hyperparameter settings from Level 4 to new training runs on all other levels. Figure 5 shows moderate degradations in performance for all models. In particular, when the hyperparameter values tuned on Level 4 are used in Level 5 training runs, none of the models reach a 99% solution rate within 1 million training steps, but WMG with factored observations reaches higher levels of performance than the other models. Broadly, these results indicate that WMG is no more sensitive to hyperparameter settings than the baseline agents.

4.4. Sokoban Environment

In order to evaluate WMGs ability to perform complex reasoning over factored observations, we apply it to the Sokoban environment (Botea et al., 2003), a challenging puzzle domain that humans solve by forward planning. To successfully complete an episode, the agent must solve a puzzle (Figure 6) by pushing the four yellow boxes onto the four red targets within 120 time steps. Boxes may not be pushed into walls or into other boxes. Since boxes cannot be pulled, many moves will render the puzzle unsolvable.

We employ the training set, test set, and action space defined in (Guez et al., 2019): Episodes are drawn from a diverse set of 900k pre-generated training puzzles. The agent’s action space is discrete, consisting of one action for movement (if not blocked) in each possible direction, plus one no-op action. The agent receives a reward of +1 for pushing a box onto a target, and -1 for pushing a box off of a target. Once all four boxes are on targets, the agent receives a bonus reward of +2, and the episode ends. We do not apply any other reward shaping, such as the per-time-step penalty of

-0.01 used by Guez et al. (2019).

Instead of image-based observations in (Guez et al., 2019), we factor the observation space as follows: Each non-wall cell is represented by a factor containing 6 binary flags specifying whether the cell is a target, whether it contains a box, and whether the cell is bounded by walls in the four directions. Information about the agent’s currently occupied cell is passed to the core node. All other cell factors are mapped to Percepts. Each Percept also receives two one-hot vectors specifying that cell’s X and Y locations relative to the agent. In addition, the core node receives a one-hot vector reporting the agent’s previous action and reward received. Compared to image-based observations, our factored space adds ego-centric information by encoding the *relative* positions of objects. The two spaces are otherwise isomorphic.

We performed a hyperparameter search on the 900k puzzle training set (Arthur Guez, 2018). After choosing the final hyperparameter configuration, we evaluated the saved models of twenty independent training runs on the 1000-puzzle test set. As shown in Fig 7, WMG learns to solve 80% of the test puzzles after 13.5 million environment interactions, while DRC (Guez et al., 2019) requires 20M interactions. Videos of WMG solving and failing at Sokoban puzzles can be viewed at <https://tinyurl.com/vdz6gdd>.

5. Conclusion and future work

We designed the *Working Memory Graph* to investigate how self-attention can improve the memory and reasoning capabilities of RL agents. In contrast to previous models, WMG can effectively leverage factored observations by encoding them into Percept vectors and applying Transformer-style self-attention. In order to represent multiple latent aspects of partially observable environments, WMG incorporates a novel form of recurrence using Concept vectors to create multiple shortcut paths of self-attention.

We compared WMG to gated RNN-based architectures (including state-of-the-art models like DRC) in three diverse

Level	1	2	3
WMG-factored	5.0	13.5	34.7
nr-WMG-factored	3.2	9.9	39.3
GRU-factored	8.0	42.6	313.9
WMG-flat	40.6	74.9	231.4
GRU-flat	36.9	55.3	188.9

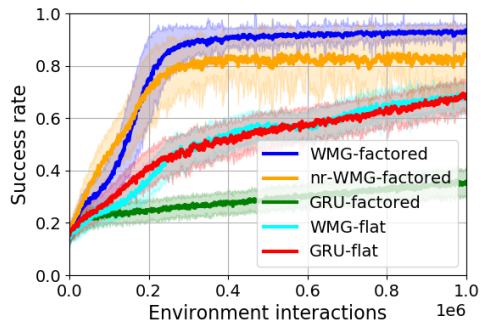


Figure 5. **Hyperparameter Sensitivity:** Sample efficiency (in thousands of environment interactions) of various model-format combinations using hyperparameters optimized for Level 4 then subsequently applied to Levels 1, 2, and 3 (left), as well as 5 (right). All model performances degrade, but WMG with factors still outperforms GRU-based models. Although none of the models reach the 99% threshold for Level 5, WMG reaches a high level of performance before the others. (See Table 1 for more details.)

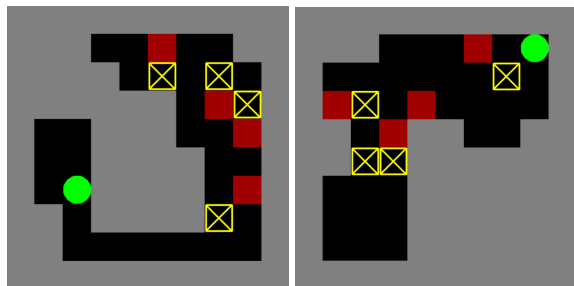


Figure 6. **Example Sokoban puzzles:** the agent (green circle) must push the boxes (yellow squares) into the red target locations.

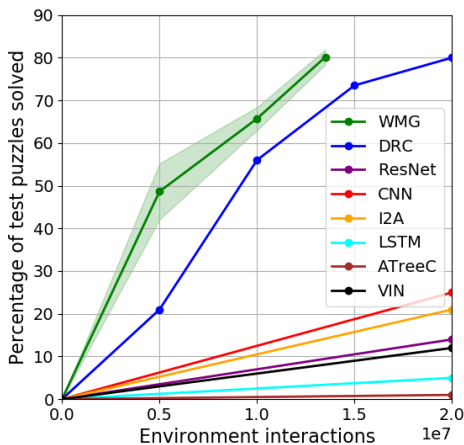


Figure 7. **Sokoban results:** 20 independent WMG agents were each trained for 13.5 million environment interactions on the 900k-puzzle training set. Cached models were subsequently evaluated on the 1000-puzzle test set. The shaded region displays one standard deviation. Results for DRC and the other baseline models are from (Guez et al., 2019).

environments featuring factored observations and complex reasoning over long-term dependencies. In these experiments, WMG outperforms competing models and demonstrates its ability to learn complex tasks in a sample-efficient manner.

We stop short of claiming state-of-the-art performance on these domains as factorizing the observation space may alter the difficulty of the task. Instead, we aim to illuminate how factored observations combined with self-attention models like WMG can yield superior learning performance.

No model is without limitations. We conclude by outlining limitations of WMG as suggestions for future work:

Flexible Concept lifetimes: In this paper, each new Concept automatically replaces the oldest. A more flexible and adaptive Concept-deletion scheme may improve WMG’s ability to model latent aspects in the environment. For instance, Concept vectors that receive more attention than others may be the ones most worth keeping around for longer. Deleting a Concept only when its recently-received attention falls below a certain threshold would allow the number of Concept vectors to fluctuate somewhat over time.

Graph edge content: As in the original Transformer, WMG applies input vectors to the nodes in its computation graph, but not to the edges between them. To better represent graph-structured data, Veličković et al. (2017) contemplated incorporating edge-specific data into Graph Attention Networks. By harnessing the richer representational abilities of graph structures over set structures, a similar extension of WMG may allow it to better model complex relations among observed and latent factors in the environment.

Memory vectors: Various forms of external memory have been proposed recently (Graves et al., 2016; Munkhdalai et al., 2019). Memory vectors retrieved from such stores could be fed to dedicated WMG *memory* nodes, in addition to the Concept and Percept nodes, to further extend the

range and flexibility of an agent’s reasoning horizon.

ACKNOWLEDGMENTS

The authors wish to thank Alekh Agarwal and Xiaodong Liu for many valuable discussions, and Felipe Frujeri for creating the Sokoban videos.

References

- Anonymous. Stabilizing transformers for reinforcement learning, 2019. URL <https://openreview.net/forum?id=SyxKrySYPr>. Under review, International Conference on Learning Representations, 2020.
- Karol Gregor Rishabh Kabra Sebastien Racaniere Theophane Weber David Raposo Adam Santoro Laurent Orseau Tom Eccles Greg Wayne David Silver Timothy Lillicrap Victor Valdes Arthur Guez, Mehdi Mirza. An investigation of model-free planning: boxoban levels. <https://github.com/deepmind/boxoban-levels/>, 2018.
- Dzmitry Bahdanau, Kyunghyun Cho, and Yoshua Bengio. Neural machine translation by jointly learning to align and translate, 2014. URL <http://arxiv.org/abs/1409.0473>. Accepted at ICLR 2015 as oral presentation.
- Adi Botea, Martin Müller, and Jonathan Schaeffer. Using abstraction for planning in sokoban. In Jonathan Schaeffer, Martin Müller, and Yngvi Björnsson (eds.), *Computers and Games*, pp. 360–375, Berlin, Heidelberg, 2003. Springer Berlin Heidelberg. ISBN 978-3-540-40031-8.
- Craig Boutilier, Raymond Reiter, Mikhail Soutchanski, and Sebastian Thrun. Decision-theoretic, high-level agent programming in the situation calculus. In *Proceedings of the Seventeenth National Conference on Artificial Intelligence and Twelfth Conference on Innovative Applications of Artificial Intelligence*, pp. 355–362. AAAI Press, 2000. ISBN 0-262-51112-6. URL <http://dl.acm.org/citation.cfm?id=647288.721273>.
- Craig Boutilier, Ray Reiter, and Bob Price. Symbolic dynamic programming for first-order mdps. In *Proceedings of the 17th International Joint Conference on Artificial Intelligence - Volume 1, IJCAI’01*, pp. 690–697, San Francisco, CA, USA, 2001. Morgan Kaufmann Publishers Inc. ISBN 1-55860-812-5, 978-1-558-60812-2. URL <http://dl.acm.org/citation.cfm?id=1642090.1642184>.
- Maxime Chevalier-Boisvert, Dzmitry Bahdanau, Salem Lahlou, Lucas Willems, Chitwan Saharia, Thien Huu Nguyen, and Yoshua Bengio. Babyai: First steps towards grounded language learning with a human in the loop. *CoRR*, abs/1810.08272, 2018. URL <http://arxiv.org/abs/1810.08272>.
- Junyoung Chung, Kyle Kastner, Laurent Dinh, Kratarth Goel, Aaron Courville, and Yoshua Bengio. A recurrent latent variable model for sequential data. In *Proceedings of the 28th International Conference on Neural Information Processing Systems - Volume 2, NIPS’15*, pp. 2980–2988, Cambridge, MA, USA, 2015. MIT Press. URL <http://dl.acm.org/citation.cfm?id=2969442.2969572>.
- Jacob Devlin, Ming-Wei Chang, Kenton Lee, and Kristina Toutanova. BERT: pre-training of deep bidirectional transformers for language understanding. *CoRR*, abs/1810.04805, 2018. URL <http://arxiv.org/abs/1810.04805>.
- Li Dong, Nan Yang, Wenhui Wang, Furu Wei, Xiaodong Liu, Yu Wang, Jianfeng Gao, Ming Zhou, and Hsiao-Wuen Hon. Unified language model pre-training for natural language understanding and generation. *CoRR*, abs/1905.03197, 2019. URL <http://arxiv.org/abs/1905.03197>.
- Anirudh Goyal, Alex Lamb, Jordan Hoffmann, Shagun Sodhani, Sergey Levine, Y. Bengio, and Bernhard Schölkopf. Recurrent independent mechanisms. *CoRR*, abs/1909.10893, 09 2019. URL <http://arxiv.org/abs/1909.10893>.
- Alex Graves, Greg Wayne, Malcolm Reynolds, Tim Harley, Ivo Danihelka, Agnieszka Grabska-Barwińska, Sergio Gómez Colmenarejo, Edward Grefenstette, Tiago Ramalho, John Agapiou, Adrià Puigdomènech Badia, Karl Moritz Hermann, Yori Zwols, Georg Ostrovski, Adam Cain, Helen King, Christopher Summerfield, Phil Blunsom, Koray Kavukcuoglu, and Demis Hassabis. Hybrid computing using a neural network with dynamic external memory. *Nature*, 538(7626):471–476, October 2016. ISSN 00280836. URL <http://dx.doi.org/10.1038/nature20101>.
- Arthur Guez, Mehdi Mirza, Karol Gregor, Rishabh Kabra, Sébastien Racanière, Théophane Weber, David Raposo, Adam Santoro, Laurent Orseau, Tom Eccles, Greg Wayne, David Silver, and Timothy P. Lillicrap. An investigation of model-free planning. *CoRR*, abs/1901.03559, 2019. URL <http://arxiv.org/abs/1901.03559>.
- Matthew J. Hausknecht and Peter Stone. Deep recurrent q-learning for partially observable mdps. *CoRR*, abs/1507.06527, 2015. URL <http://arxiv.org/abs/1507.06527>.
- Kaiming He, Xiangyu Zhang, Shaoqing Ren, and Jian Sun. Delving deep into rectifiers: Surpassing human-level performance on imagenet classification. *CoRR*,

- abs/1502.01852, 2015. URL <http://arxiv.org/abs/1502.01852>.
- Sepp Hochreiter and Jürgen Schmidhuber. Long short-term memory. *Neural Comput.*, 9(8):1735–1780, November 1997. ISSN 0899-7667. doi: 10.1162/neco.1997.9.8.1735. URL <http://dx.doi.org/10.1162/neco.1997.9.8.1735>.
- Leslie Pack Kaelbling, Michael L. Littman, and Anthony R. Cassandra. Planning and acting in partially observable stochastic domains. *Artif. Intell.*, 101(1-2):99–134, May 1998. ISSN 0004-3702. doi: 10.1016/S0004-3702(98)00023-X. URL [http://dx.doi.org/10.1016/S0004-3702\(98\)00023-X](http://dx.doi.org/10.1016/S0004-3702(98)00023-X).
- Diederik P. Kingma and Jimmy Ba. Adam: A method for stochastic optimization, 2014. URL <http://arxiv.org/abs/1412.6980>. 3rd International Conference for Learning Representations, San Diego, 2015.
- Yinhan Liu, Myle Ott, Naman Goyal, Jingfei Du, Mandar Joshi, Danqi Chen, Omer Levy, Mike Lewis, Luke Zettlemoyer, and Veselin Stoyanov. Roberta: A robustly optimized BERT pretraining approach. *CoRR*, abs/1907.11692, 2019. URL <http://arxiv.org/abs/1907.11692>.
- George A. Miller. The magical number seven, plus or minus two: Some limits on our capacity for processing information. *The Psychological Review*, 63(2):81–97, March 1956. URL <http://www.musanim.com/miller1956/>.
- Volodymyr Mnih, Koray Kavukcuoglu, David Silver, Andrei A. Rusu, Joel Veness, Marc G. Bellemare, Alex Graves, Martin Riedmiller, Andreas K. Fidjeland, Georg Ostrovski, Stig Petersen, Charles Beattie, Amir Sadik, Ioannis Antonoglou, Helen King, Dharshan Kumaran, Daan Wierstra, Shane Legg, and Demis Hassabis. Human-level control through deep reinforcement learning. *Nature*, 518(7540):529–533, February 2015. ISSN 00280836. URL <http://dx.doi.org/10.1038/nature14236>.
- Volodymyr Mnih, Adrià Puigdomènech Badia, Mehdi Mirza, Alex Graves, Timothy P. Lillicrap, Tim Harley, David Silver, and Koray Kavukcuoglu. Asynchronous methods for deep reinforcement learning. In *Proceedings of the 33rd International Conference on Machine Learning (ICML)*, pp. 1928–1937, 2016.
- Tsendsuren Munkhdalai, Alessandro Sordani, Tong Wang, and Adam Trischler. Metalearned neural memory. *CoRR*, abs/1907.09720, 2019. URL <http://arxiv.org/abs/1907.09720>.
- Junhyuk Oh, Valliappa Chockalingam, Satinder Singh, and Honglak Lee. Control of memory, active perception, and action in minecraft. In *Proceedings of the 33rd International Conference on International Conference on Machine Learning - Volume 48, ICML’16*, pp. 2790–2799. JMLR.org, 2016. URL <http://dl.acm.org/citation.cfm?id=3045390.3045684>.
- Ethan Perez, Florian Strub, Harm de Vries, Vincent Dumoulin, and Aaron C. Courville. Film: Visual reasoning with a general conditioning layer. *CoRR*, abs/1709.07871, 2017. URL <http://arxiv.org/abs/1709.07871>.
- Stuart Russell and Peter Norvig. *Artificial Intelligence: A Modern Approach*. Prentice Hall Press, Upper Saddle River, NJ, USA, 3rd edition, 2009. ISBN 0136042597, 9780136042594.
- Adam Santoro, Ryan Faulkner, David Raposo, Jack W. Rae, Mike Chrzanowski, Theophane Weber, Daan Wierstra, Oriol Vinyals, Razvan Pascanu, and Timothy P. Lillicrap. Relational recurrent neural networks. *CoRR*, abs/1806.01822, 2018. URL <http://arxiv.org/abs/1806.01822>.
- Max-Philipp B. Schrader. gym-sokoban. <https://github.com/mpSchrader/gym-sokoban>, 2018.
- Ilya Sutskever, Oriol Vinyals, and Quoc V. Le. Sequence to sequence learning with neural networks. In *Proceedings of the 27th International Conference on Neural Information Processing Systems - Volume 2, NIPS’14*, pp. 3104–3112, Cambridge, MA, USA, 2014. MIT Press. URL <http://dl.acm.org/citation.cfm?id=2969033.2969173>.
- Ashish Vaswani, Noam Shazeer, Niki Parmar, Jakob Uszkoreit, Llion Jones, Aidan N. Gomez, Lukasz Kaiser, and Illia Polosukhin. Attention is all you need. *CoRR*, abs/1706.03762, 2017. URL <http://arxiv.org/abs/1706.03762>.
- Petar Veličković, Guillem Cucurull, Arantxa Casanova, Adriana Romero, Pietro Liò, and Yoshua Bengio. Graph attention networks. *CoRR*, abs/1710.10903, 2017. URL <http://arxiv.org/abs/1710.10903>.
- Oriol Vinyals, Igor Babuschkin, Wojciech M Czarnecki, Michaël Mathieu, Andrew Dudzik, Junyoung Chung, David H Choi, Richard Powell, Timo Ewalds, Petko Georgiev, et al. Grandmaster level in starcraft ii using multi-agent reinforcement learning. *Nature*, pp. 1–5, 2019.

Vinicius Zambaldi, David Raposo, Adam Santoro, Victor Bapst, Yujia Li, Igor Babuschkin, Karl Tuyls, David Reichert, Timothy Lillicrap, Edward Lockhart, Murray Shanahan, Victoria Langston, Razvan Pascanu, Matthew Botvinick, Oriol Vinyals, and Peter Battaglia. Deep reinforcement learning with relational inductive biases, 2019.

Appendices

A. Pathfinding Task Details

The Pathfinding graph is constrained to be a polytree (singly connected, directed acyclic graph) at each step of an episode, as outlined in Algorithm 1.

Algorithm 1 Pathfinding Episode Dynamics

Input: pattern size D , max graph size N .
Initialize $Graph = empty$.
Add a node with random pattern $\in (-1, +1)^D$.
 $AddPattern = true$.
repeat
 Input: agent $Action$.
 $Reward = 0$.
 $Done = false$.
 if $AddPattern$ is true **then**
 // Construction step.
 if $size(Graph) > 1$ and $Action == Target$ **then**
 $Reward = 1$.
 end if
 if $size(Graph) == N$ **then**
 $Done = true$.
 else
 Choose random node A from the Graph.
 Add node B with random pattern $\in (-1, +1)^D$.
 Link A and B in a random direction.
 $Observation = A, B, 0$.
 $AddPattern = false$.
 end if
 else
 // Quiz step.
 Choose random $Target \in (true, false)$.
 repeat
 Choose random nodes X and Y .
 $PathExists = path$ exists from X to Y .
 until $PathExists == Target$
 $Observation = X, Y, 1$.
 $AddPattern = true$.
 end if
 Output: $Reward, Observation, Done$
until $Done$ is true

The hand-coded baseline agent is configured with a depth parameter n . As new pattern pairs are revealed on graph-construction time steps, this agent maintains a growing vector of all patterns seen, along with a growing matrix of directed path lengths from every observed pattern to every other. A path length of zero in this matrix indicates that no path exists from the first pattern to the second. On each quiz step, the agent looks up from the matrix the path length len for the ordered pair of patterns in the observation. If

$0 < len \leq n$, the agent chooses the *yes* action. Otherwise, the agent chooses the *no* action.

B. Sokoban Attention Maps

To aid visualization of WMG’s inner operations, many of the videos at <https://tinyurl.com/vdz6gdd> display white squares with areas proportional to the per-step attention probabilities applied by WMG’s core node to all nodes in the preceding layer. These probabilities are summed over all attention heads, and over all layer pairs above the lowest. Attention applied to the single (in this task) Concept node is represented by the white square in the upper-left cell. Our implementation of the Sokoban environment is based in part on that of Schrader (2018).

C. Hyperparameter Tuning Procedures

C.1. DGD

In this work, all hyperparameters were tuned by a guided form of random search that we call *Distributed Grid Descent* (DGD). It is designed to address the challenges posed by large numbers of hyperparameters (10-20), and the high variance among independent training runs using the same hyperparameter configuration that is often observed in deep RL experiments. DGD tackles these challenges by steering the random selection of configurations to be tested towards a robust basin, defined as a configuration for which modification of any individual hyperparameter setting by one step higher or lower results in worse performance in expectation. In addition, DGD is designed to run on multiple processes on potentially many machines with no central point of control.

To describe the DGD algorithm, we first define the following terms:

Tuning metric: A user-defined value calculated per training run for which higher is better, such as reward or success rate, or negative regret, etc.

Run result: A completed runs hyperparameter configuration and final tuning metric.

Run set: A single hyperparameter configuration, along with any available run results for that configuration.

Count(run set): The number of runs in a run set.

Metric(run set): The mean (or median) of the run metrics in a run set.

Basin: A collection of run sets sharing similar configurations.

Count(basin): The maximum *Count* of all run sets in the basin.

The operation of each DGD worker process is described by Algorithm 2.

Algorithm 2 Distributed Grid Descent

Input: Set of hyperparameters H , each having a discrete, ordered set of possible values.

Input: Maximum number of training steps N per run.

repeat

Download any new run results.

if no results so far **then**

Choose a random configuration C from the grid defined by H .

else

Identify the run set S with the highest *Metric*.

Initialize basin B to contain only S .

Expand B by adding all possible run sets whose configurations differ from that of S by one step in exactly one hyperparameter setting.

Calculate a ceiling $M = \text{Count}(B) + 1$.

Weight each run set x in B by $M - \text{Count}(x)$.

Sample a random run set S' from B according to their weights.

Choose the configuration C from S' .

end if

Perform one training run of N steps using C .

Calculate the runs *Metric*.

Log the run result to shared storage.

until terminated by user.

Periodically throughout the DGD search, the *best* run set is determined by a function of each run set’s *Metric* and *Count*, to filter out high-variance run sets having high average scores but relatively few runs. After the best run set remains unchanged for some period, the DGD search is terminated, and the best run sets hyperparameter configuration is taken as the output of the search. To minimize the effects of local optima, the best run set can be chosen from a number of independent DGD searches.

C.2. Application of DGD

For the Pathfinding and BabyAI experiments, we ran five parallel DGD hyperparameter searches to convergence for each model, using the full number of training steps per run for the given experiment, and chose the best run set’s hyperparameter configuration after convergence.

For WMG on Sokoban, we performed 60 DGD searches using training runs of 1.5M steps, with puzzle completion success rate as the tuning metric. After these searches converged, we selected the best 25 configurations based on the training set results, and initiated 20 open-ended training runs for each configuration.

After 10M steps of training for each configuration, we se-

lected the single best hyperparameter configuration based on its running performance on the training set. We then branched this configuration into 10 sets of runs by starting to anneal the learning rate every 100k steps using one of 10 separate values of gamma ranging from 0.6 to 0.98.

On the day of paper submission, at the point where each of these final models had been trained for 13.5 million environment interactions, we selected the best performing configuration based on training set results. Then we cracked open the Sokoban test set, and used it to evaluate this configurations final 20 models, as well as its intermediate models that were cached at 5M and 10M steps of training.

All experiments were performed on Linux virtual machines in a public cloud. The VMs featured Intel 2.6GHz Xeon E5 2667 v3 processors with 8 virtual CPUs, and no GPUs.

D. Supplemental Tables

Table 2. Fixed settings and options used for all experiments, except for the replicated baselines in Table 14.

Settings and options	Values
Dropout	None
Learning rate schedule	Constant learning rate, except where noted
Non-linearities	ReLU, tanh
Parallel training workers	1
Optimizer	Adam (Kingma & Ba, 2014)
Parameter initialization, biases	0
Parameter initialization, non-bias weights	Kaiming uniform (He et al., 2015)
Reward shaping	None
Training algorithm	Advantage actor-critic (Mnih et al., 2016)
Weight decay regularization	None

Table 3. Tuned hyperparameter settings for Pathfinding experiments of 20M steps.

	WMG	nr-WMG	GRU
Actor-critic hidden layer size	128	128	512
Actor-critic t_{max}	16	16	16
Adam eps	1e-06	1e-08	1e-08
Discount factor γ	0.5	0.6	0.5
Entropy term strength β	0.01	0.005	0.02
Gradient clipping threshold	16.0	16.0	4.
GRU observation embedding size	-	-	256
GRU size	-	-	384
Learning rate	0.00016	0.00016	0.0001
Reward scale factor	2.0	1.0	0.5
WMG attention head size	12	16	-
WMG attention heads	6	6	-
WMG Concept nodes	16	0	-
WMG Concept size	128	-	-
WMG hidden layer size	12	32	-
WMG layers	4	4	-

Table 4. Tuned hyperparameter settings for Pathfinding experiments of 1M steps.

	WMG	nr-WMG	GRU
Actor-critic hidden layer size	2880	256	5760
Actor-critic t_{max}	16	16	16
Adam eps	1e-04	1e-12	1e-06
Discount factor γ	0.5	0.5	0.5
Entropy term strength β	0.005	0.05	0.1
Gradient clipping threshold	256.0	4.0	32.
GRU observation embedding size	-	-	1024
GRU size	-	-	256
Learning rate	0.00004	0.00016	0.0001
Reward scale factor	4.0	2.0	2.0
WMG attention head size	90	90	-
WMG attention heads	4	1	-
WMG Concept nodes	6	0	-
WMG Concept size	256	-	-
WMG hidden layer size	8	16	-
WMG layers	3	5	-

Table 5. Tuned hyperparameter settings for BabyAI Level 1 - GoToObj.

	WMG factored	nr-WMG factored	GRU factored	WMG flat	GRU flat	CNN+GRU native 7x7x3
Actor-critic hidden layer size	2048	4096	4096	4096	2048	512
Actor-critic t_{max}	1	1	6	16	4	6
Adam eps	0.0001	1e-08	1e-08	1e-10	0.0001	1e-10
CNN hidden channel size 1	-	-	-	-	-	16
CNN hidden channel size 2	-	-	-	-	-	40
CNN hidden channel size 3	-	-	-	-	-	192
Discount factor γ	0.98	0.9	0.7	0.6	0.9	0.8
Entropy term strength β	0.002	0.05	0.01	0.005	0.02	0.02
Gradient clipping threshold	256.0	1024.0	512.0	512.0	128.0	128.0
GRU observation embed size	-	-	1024	-	512	512
GRU size	-	-	96	-	512	96
Learning rate	0.0001	4e-05	0.0004	0.0001	0.0001	0.0004
Reward scale factor	4.0	32.0	32.0	8.0	32.0	8.0
WMG attention head size	24	16	-	16	-	-
WMG attention heads	4	10	-	12	-	-
WMG Concept nodes	1	0	-	1	-	-
WMG Concept size	64	-	-	256	-	-
WMG hidden layer size	64	64	-	32	-	-
WMG layers	4	4	-	1	-	-

Working Memory Graphs

Table 6. Tuned hyperparameter settings for BabyAI Level 2 - GoToRedBallGrey.

	WMG factored	nr-WMG factored	GRU factored	WMG flat	GRU flat	CNN+GRU native 7x7x3
Actor-critic hidden layer size	4096	2048	4096	4096	4096	64
Actor-critic t_{max}	8	6	16	1	1	1
Adam eps	1e-06	1e-08	1e-10	1e-10	1e-06	0.0001
CNN hidden channel size 1	-	-	-	-	-	12
CNN hidden channel size 2	-	-	-	-	-	24
CNN hidden channel size 3	-	-	-	-	-	192
Discount factor γ	0.8	0.9	0.8	0.9	0.9	0.95
Entropy term strength β	0.01	0.02	0.01	0.005	0.005	0.02
Gradient clipping threshold	1024.0	512.0	1024.0	128.0	64.0	64.0
GRU observation embed size	-	-	4096	-	2048	256
GRU size	-	-	96	-	512	64
Learning rate	0.0001	0.00025	0.0001	2.5e-05	2.5e-05	0.0004
Reward scale factor	8.0	4.0	4.0	4.0	4.0	2.0
WMG attention head size	64	48	-	64	-	-
WMG attention heads	4	1	-	3	-	-
WMG Concept nodes	1	0	-	8	-	-
WMG Concept size	32	-	-	64	-	-
WMG hidden layer size	16	24	-	384	-	-
WMG layers	3	3	-	1	-	-

Table 7. Tuned hyperparameter settings for BabyAI Level 3 - GoToRedBall.

	WMG factored	nr-WMG factored	GRU factored	WMG flat	GRU flat	CNN+GRU native 7x7x3
Actor-critic hidden layer size	4096	2048	4096	4096	4096	4096
Actor-critic t_{max}	1	2	3	1	2	3
Adam eps	1e-12	0.0001	1e-06	0.0001	1e-06	0.01
CNN hidden channel size 1	-	-	-	-	-	12
CNN hidden channel size 2	-	-	-	-	-	40
CNN hidden channel size 3	-	-	-	-	-	192
Discount factor γ	0.95	0.9	0.9	0.9	0.9	0.9
Entropy term strength β	0.1	0.05	0.1	0.05	0.02	0.05
Gradient clipping threshold	128.0	128.0	128.0	128.0	32.0	32.0
GRU observation embed size	-	-	2048	-	4096	256
GRU size	-	-	192	-	512	64
Learning rate	2.5e-05	6.3e-05	6.3e-05	2.5e-05	2.5e-05	0.0004
Reward scale factor	8.0	4.0	8.0	8.0	4.0	4.0
WMG attention head size	128	32	-	24	-	-
WMG attention heads	2	8	-	12	-	-
WMG Concept nodes	2	0	-	16	-	-
WMG Concept size	128	-	-	256	-	-
WMG hidden layer size	64	32	-	128	-	-
WMG layers	4	4	-	1	-	-

Working Memory Graphs

Table 8. Tuned hyperparameter settings for BabyAI Level 4 - GoToLocal.

	WMG factored	nr-WMG factored	GRU factored	WMG flat	GRU flat
Actor-critic hidden layer size	2048	2048	1024	512	4096
Actor-critic t_{max}	6	3	3	6	4
Adam eps	1e-12	0.01	1e-06	1e-08	1e-12
Discount factor γ	0.5	0.6	0.95	0.5	0.9
Entropy term strength β	0.1	0.1	0.1	0.02	0.02
Gradient clipping threshold	512.0	512.0	256.0	256.0	512.0
GRU observation embed size	-	-	1024	-	512
GRU size	-	-	128	-	96
Learning rate	6.3e-05	0.0001	4e-05	2.5e-05	4e-05
Reward scale factor	32.0	16.0	8.0	16.0	2.0
WMG attention head size	128	64	-	24	-
WMG attention heads	2	4	-	16	-
WMG Concept nodes	8	0	-	16	-
WMG Concept size	32	-	-	64	-
WMG hidden layer size	32	48	-	16	-
WMG layers	4	3	-	2	-

Table 9. Tuned hyperparameter settings for BabyAI Level 5 - PickupLoc.

	WMG factored	nr-WMG factored
Actor-critic hidden layer size	512	2048
Actor-critic t_{max}	12	12
Adam eps	1e-10	1e-10
Discount factor γ	0.7	0.8
Entropy term strength β	0.02	0.05
Gradient clipping threshold	512.0	512.0
Learning rate	0.0001	6.3e-05
Reward scale factor	8.0	8.0
WMG attention head size	24	48
WMG attention heads	10	6
WMG Concept nodes	8	0
WMG Concept size	32	-
WMG hidden layer size	128	96
WMG layers	2	2

Table 10. Tuned hyperparameter settings for WMG on Sokoban. The resulting model contained 4,508,182 trainable parameters. (The Pathfinding and BabyAI experiments used very similar hyperparameter ranges, so their ranges are not listed separately.)

	Tuned value	Range considered
Reward per step	0	0, -0.01, -0.01
Reward on success	2	2, 5, 10, 15, 20
Actor-critic hidden layer size	2880	180, 256, 360, 512, 720, 1024, 1440, 2048, 2880, 4096, 5760
Actor-critic t_{max}	4	4, 6, 8, 12, 16, 24, 32, 48, 64, 96, 120
Adam eps	1e-10	1e-4, 1e-6, 1e-8, 1e-10
Discount factor γ	0.995	0.7, 0.8, 0.9, 0.95, 0.98, 0.99, 0.995, 0.998
Entropy term strength β	0.02	0.002, 0.005, 0.01, 0.02, 0.05
Gradient clipping threshold	512.0	64, 128, 256, 512, 1024, 2048
Learning rate	1.6e-5	6.3e-6, 1e-5, 1.6e-5, 2.5e-5, 4e-5, 6.3e-5, 1e-4, 1.6e-4
Learning rate annealing γ	0.93	0.60, 0.64, 0.68, 0.72, 0.76, 0.80, 0.84, 0.88, 0.93, 0.98
Reward scale factor	4	0.5, 1, 2, 4, 8
WMG attention head size	32	8, 12, 16, 24, 32, 45, 64, 90, 128
WMG attention heads	8	6, 8, 10, 12, 16, 20
WMG Concept nodes	1	1, 2, 3, 4, 6, 8, 10, 12, 16, 20
WMG Concept size	2048	90, 128, 180, 256, 360, 512, 720, 1024, 1440, 2048
WMG hidden layer size	8	6, 8, 12, 16, 24, 32, 45, 64, 90, 128
WMG layers	10	5, 6, 7, 8, 9, 10, 11, 12, 13

Table 11. Additional details for the Pathfinding experimental results in Figure 3 (right).

Models & algorithms	Final performance	Trainable parameters	Training speed
<i>Depth-(n-1)</i> baseline	100.0% of reward		
<i>Depth-3</i> baseline	99.7% of reward		
<i>Depth-2</i> baseline	97.6% of reward		
<i>Depth-1</i> baseline	86.9% of reward		
nr-WMG, full-history	99.6% of reward	204,963	96 steps/sec
WMG	99.6% of reward	132,507	91 steps/sec
GRU	94.7% of reward	1,139,459	291 steps/sec

Table 12. Number of trainable parameters, in thousands, for the BabyAI models in Table 1.

BabyAI level	WMG	nr-WMG	GRU	WMG	GRU	CNN+GRU
	factored	factored	factored	flat	flat	native 7x7x3
1 - GoToObj	636	1,864	1,572	2,053	4,170	393
2 - GoToRedBallGrey	2,997	258	3,723	2,116	10,075	140
3 - GoToRedBall	3,418	2,217	3,749	3,229	15,126	709
4 - GoToLocal	2,235	1,960	1,137	2,022	1,479	—
5 - PickupLoc	879	2,007	—	—	—	—

Table 13. Training steps per second on a fixed machine, for the BabyAI models in Table 1.

BabyAI level	WMG	nr-WMG	GRU	WMG	GRU	CNN+GRU
	factored	factored	factored	flat	flat	native 7x7x3
1 - GoToObj	38	28	146	111	86	149
2 - GoToRedBallGrey	58	113	147	35	18	88
3 - GoToRedBall	18	32	78	25	20	87
4 - GoToLocal	44	48	132	54	134	—
5 - PickupLoc	81	84	—	—	—	—

Table 14. BabyAI baseline agent sample efficiencies, defined as the amount of training (in either episodes or environment interaction steps) required for the agent to solve 99% of random episodes within 64 steps. The published results are the means of the min & max RL sample efficiencies reported in Table 3 of [Chevalier-Boisvert et al. \(2018\)](#). The replicated results are the medians over 10 training runs, using the code and default hyperparameter settings from the open source release of the BabyAI baseline agent. All numbers are in thousands.

BabyAI level	Instruction template	Published (episodes)	Replicated (episodes)	Replicated (interactions)
1 - GoToObj	GO TO color object	—	19	333
2 - GoToRedBallGrey	GO TO RED BALL	16	16	282
3 - GoToRedBall	GO TO RED BALL	272	283	3,674
4 - GoToLocal	GO TO color object	971	1,064	16,422
5 - PickupLoc	PICK UP color object loc	2,977	1,557	25,574